Mouse model of hematogenous implant-related *Staphylococcus aureus* biofilm infection reveals therapeutic targets

Yu Wang[a], Lily I. Cheng[b], David R. Helfer[a], Alyssa G. Ashbaugh[a], Robert J. Miller[a], Alexander J. Tzomides[a], John M. Thompson[c], Roger V. Ortines[a], Andrew S. Tsai[a], Haiyun Liu[a], Carly A. Dillen[a], Nathan K. Archer[a], Taylor S. Cohen[d], Christine Tkaczyk[d], C. Kendall Stover[d], Bret R. Sellman[d], and Lloyd S. Miller[a,c,e,f,1]

[a]Department of Dermatology, Johns Hopkins University School of Medicine, Baltimore, MD 21231; [b]Department of Translational Science, Medimmune, LLC, Gaithersburg, MD 20878; [c]Department of Orthopaedic Surgery, Johns Hopkins University School of Medicine, Baltimore, MD 21287; [d]Department of Infectious Disease, Medimmune, LLC, Gaithersburg, MD 20878; [e]Division of Infectious Diseases, Department of Medicine, Johns Hopkins University School of Medicine, Baltimore, MD 21287; and [f]Department of Materials Science and Engineering, Johns Hopkins University, Baltimore, MD 21218

Edited by Jeff F. Miller, University of California, Los Angeles, CA, and approved May 24, 2017 (received for review February 28, 2017)

Infection is a major complication of implantable medical devices, which provide a scaffold for biofilm formation, thereby reducing susceptibility to antibiotics and complicating treatment. Hematogenous implant-related infections following bacteremia are particularly problematic because they can occur at any time in a previously stable implant. Herein, we developed a model of hematogenous infection in which an orthopedic titanium implant was surgically placed in the legs of mice followed 3 wk later by an i.v. exposure to *Staphylococcus aureus*. This procedure resulted in a marked propensity for a hematogenous implant-related infection comprised of septic arthritis, osteomyelitis, and biofilm formation on the implants in the surgical legs compared with sham-operated surgical legs without implant placement and with contralateral nonoperated normal legs. Neutralizing human monoclonal antibodies against α-toxin (AT) and clumping factor A (ClfA), especially in combination, inhibited biofilm formation in vitro and the hematogenous implant-related infection in vivo. Our findings suggest that AT and ClfA are pathogenic factors that could be therapeutically targeted against *S. aureus* hematogenous implant-related infections.

hematogenous | implant | *Staphylococcus aureus* | biofilm | orthopedic

Infections of implantable medical devices are associated with bacterial biofilms that form on the implanted foreign materials and are impervious to antibiotic and immune cell penetration (1, 2), leading to chronic and difficult-to-treat infections (3, 4). In particular, the treatment of prosthetic joint infections (PJI) (i.e., infection of knee and hip joint prostheses) is exceedingly difficult because it typically involves reoperations to remove the infected prosthesis, prolonged courses of systemic antibiotics, and delayed reimplantation of a new prosthesis, all of which contribute to extended disability and rehabilitation and increased morbidity, mortality, and healthcare costs (5, 6). Most PJI and other implant-related infections are thought to occur by invading bacteria during surgery or in the immediate postoperative period (7, 8). However, hematogenous infections, which represent up to 20% of PJI, are especially problematic because they can occur at any time after implantation by bacteria from a remote source of infection or exposure seeding a previously well-functioning prosthesis through the bloodstream (9–11). *Staphylococcus aureus* is a particularly clinically relevant pathogen because it is the most common cause of PJI in humans (12, 13), and *S. aureus* bacteremia results in a hematogenous PJI in 30–40% of patients with joint prostheses in place at the time of *S. aureus* bacteremia (9, 11, 14). Furthermore, community-associated methicillin-resistant *S. aureus* (CA-MRSA) clinical isolates are increasingly becoming resistant to antibiotics (15, 16), underscoring the unmet clinical need for therapeutic alternatives to conventional antibiotics.

In individuals with implantable medical devices, systemic antibiotics are currently used as prophylactic therapy against hematogenous implant infections before medical and surgical procedures associated with a transient bacteremia (e.g., colonoscopies and urologic and dental procedures) (17–19). A major concern is that the efficacy of antibiotic prophylaxis has been declining because of the increasing emergence of multidrug resistant bacteria (20). Furthermore, the impact of broad-spectrum antibiotics on the beneficial microbiota can also be a risk factor for other infections and inflammatory diseases, and antibiotic stewardship programs are aiming to reduce overall antibiotic use (21). Thus, a greater understanding of the bacterial pathologic mechanisms of hematogenous implant infections is essential to develop new, alternative therapies for prevention or treatment.

Prior preclinical models of PJI or orthopedic implant infections have involved direct insertion of an implant with bacteria already adherent to its surface (22, 23), direct inoculation of bacteria at the surgical site of an implant (24–26), or bacteremia resulting in septic arthritis in the absence of an implant (27, 28). Although each of these models has features of a hematogenous implant infection, they do not fully recapitulate the spread of the

Significance

Hematogenous implant-related infections are an important clinical problem because bacteria spread from the bloodstream to a previously well-functioning implant and result in infectious complications and failure of a medical device or prosthesis. To study these infections, we developed a preclinical animal model of a *Staphylococcus aureus* hematogenous implant infection with the capability to monitor noninvasively and longitudinally the dissemination of the bacteria from the blood to a surgically placed orthopedic implant. Using this model, α-toxin and clumping factor A were identified as key factors that contributed to the pathogenesis of these infections by promoting biofilm formation. Finally, neutralizing antibodies against these factors provided a targeted, nonantibiotic alternative approach to help prevent these difficult-to-treat and costly infections.

Author contributions: Y.W., T.S.C., C.T., C.K.S., B.R.S., and L.S.M. designed research; Y.W., L.I.C., D.R.H., A.G.A., R.J.M., A.J.T., J.M.T., R.V.O., A.S.T., H.L., C.A.D., and N.K.A. performed research; T.S.C., C.T., C.K.S., and B.R.S. contributed new reagents/analytic tools; Y.W., L.I.C., D.R.H., A.G.A., R.J.M., A.J.T., J.M.T., R.V.O., A.S.T., H.L., C.A.D., N.K.A., T.S.C., C.T., C.K.S., B.R.S., and L.S.M. analyzed data; and Y.W., T.S.C., C.T., C.K.S., B.R.S., and L.S.M. wrote the paper.

Conflict of interest statement: L.S.M. has received grant support from MedImmune, LLC for the work reported in this paper; grant support from Pfizer, Regeneron, and the Chan Soon-Shiong Nanthealth Foundation; and consulting fees from Noveome Biotherapeutics and the Chan Soon-Shiong Nanthealth Foundation that are unrelated to the work reported in this paper. L.I.C., T.S.C., C.T., C.K.S., and B.R.S. are associated with MedImmune, LLC, a subsidiary of AstraZeneca, and may hold AstraZeneca stock.

This article is a PNAS Direct Submission.

[1]To whom correspondence should be addressed. Email: lloydmiller@jhmi.edu.

bacteria from the bloodstream to the site of an implant. To the best of our knowledge, two prior preclinical models of hematogenous orthopedic implant infections in rabbits (29) and rats (30) have described the hematogenous spread of infection to the implant and surrounding bone and joint tissue at static time points but have not investigated the temporal and spatial dynamics of the infection over time or determined relevant pathogenic factors.

Therefore, we chose to develop a mouse model of a hematogenous orthopedic implant infection using a bioluminescent CA-MRSA strain in conjunction with in vivo whole-animal optical imaging to monitor the hematogenous infection noninvasively and longitudinally and to identify specific virulence factors for potential therapeutic targets.

Results

Development of a Model of Hematogenous Implant Infection. To study a hematogenous implant infection beginning with bacteremia and resulting in an implant infection, we combined surgical placement of an orthopedic implant, bioluminescent bacteria, and in vivo whole-animal bioluminescence imaging (BLI) techniques. We did so by first placing an orthopedic-grade titanium Kirschner wire (K-wire) into the right femurs of C57BL/6 mice with the end protruding into the knee joint using aseptic surgical technique (Fig. 1*A*). The groups of mice were infected i.v. 21 d post surgery, after the sterile inflammation caused by the surgical procedure had resolved, with one of three different inocula (1×10^6, 5×10^6, and 1×10^7 cfu) of a stably bioluminescent CA-MRSA strain, SAP231, and the infection was monitored with in vivo BLI on days 0, 3, 7, 14, 21, and 28 post inoculation. SAP231 has virulence similar to its parent NRS384 strain, which is a CA-MRSA USA300 strain previously isolated from a major skin and soft tissue infection outbreak (31). At early time points (3–14 d post inoculation), the BLI signals could be visualized in internal organs, especially in the kidneys and bladder, of mice that had received the 5×10^6 and 1×10^7 cfu inocula (Fig. 1*B*). By day 28 post inoculation, all three inocula resulted in the accumulation of BLI signals in the leg with the surgical implant [hereafter, the "(+) implant surgical leg"] with residual in vivo BLI signals in the bladder. In addition, the percentage of mice with BLI signal in the (+) implant surgical leg correlated with the amount of bacteria inoculated, because the percentage was significantly higher with the 1×10^7 cfu inoculum than with the 1×10^6 or 5×10^6 cfu inocula on days 14–28 ($P < 0.05$) (Fig. 1*C*). At day 28, mice were killed, and in vivo BLI was performed on internal organs as well as the (+) implant surgical legs and the contralateral nonsurgical legs (Fig. 1*D*). With all inocula, and particularly with the 1×10^7 cfu inoculum, BLI signals were seen in one (or both) kidneys and in most of the (+) implant surgical legs. Variable BLI signals were also seen in the liver and contralateral surgical legs, but no BLI signals were seen in the heart or spleen. The 1×10^7 cfu inoculum was selected for use in all subsequent experiments because it resulted in a higher percentage of BLI signals in the (+) implant surgical leg than the other inocula.

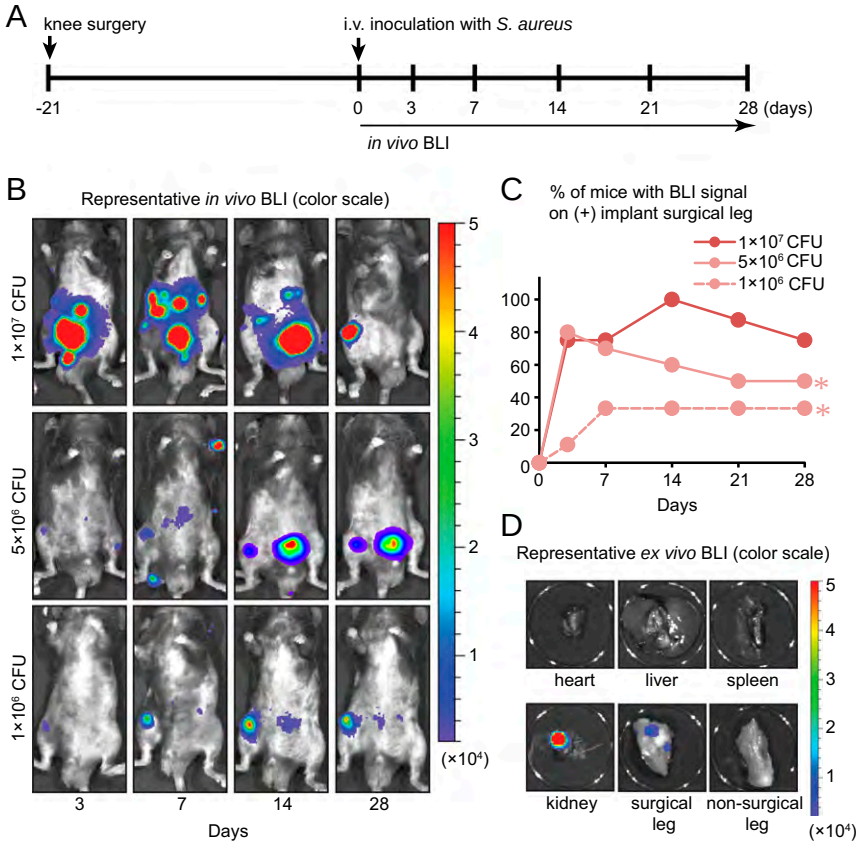

Fig. 1. Model of hematogenous implant infection. (*A*) Timeline of hematogenous infection of an orthopedic implant. (*B*) Representative images of in vivo BLI signals on a color scale overlaid on a grayscale photograph of mice with different *S. aureus* inocula. (*C*) Percentage of mice with detectable BLI signal from the (+) implant surgical leg with three different *S. aureus* inocula. (*D*) Representative images of ex vivo BLI signal from the organs and legs harvested on day 28 from mice inoculated with 1×10^7 cfu. Results are representative (*B* and *D*) or a compilation (*C*) of two independent experiments ($n = 8$–9 mice per group). *$P < 0.05$, 1×10^7 cfu vs. 1×10^6 or 5×10^6 cfu groups, as measured by a two-way ANOVA (performed on days 14–28).

In prior models of septic arthritis (in the absence of surgery or an implant), an i.v. *S. aureus* challenge had an increased propensity to spread to the knee joints of mice (27, 28). To evaluate the propensity for the hematogenous infection to spread to the knee joints of mice in the presence and absence of an implant, we used our model of hematogenous orthopedic implant infection and evaluated BLI signals from (*i*) the (+) implant surgical leg, (*ii*) the (−) implant surgical leg that had the identical surgical procedure performed but without the placement of an implant, and (*iii*) the respective nonsurgical contralateral leg (Fig. 2).

The percentage of mice with BLI signals on days 3–28 ($P < 0.05$) and the quantified in vivo BLI signals from the (+) implant surgical legs on days 7–28 ($P < 0.05$) were significantly higher than in the (−) implant surgical legs or nonsurgical legs (Fig. 2 *A* and *B*). To confirm these results obtained with in vivo BLI, ex vivo cfu were obtained from homogenized bone and joint tissue specimens on day 28 (Fig. 2*C*). The (+) implant surgical legs had significantly greater ex vivo cfu than the (−) implant surgical legs or nonsurgical legs, whereas there was no significant difference in ex vivo cfu between the (−) implant surgical legs and nonsurgical legs. Therefore, the presence of the implant resulted in a marked propensity for a hematogenous infection compared with the (−) implant surgical legs or the nonsurgical legs. To evaluate the propensity of infection further, we determined the numbers of mice with (+) and without (−) implant placement in which ex vivo cfu present were in the surgical and nonsurgical legs; these data are presented in a Euler Diagram (Fig. 2*D*). The number of mice with an infection in the surgical leg in the (+) implant group was nearly double the number of mice with an infection in the surgical leg in the (−) implant group (21 vs. 12, $P < 0.05$). Taken together, these results show that the presence of the implant was a major determinant of the propensity for hematogenous infection.

Histopathology of the Hematogenous Implant Infection. To evaluate the location of the biofilm formation on the implant and the infection in the surrounding tissue and bone, the implants and bone/joint specimens were harvested on day 28, and the implants were stained with a live/dead bacterial stain. The green (live and dead bacteria) and red (dead bacteria) fluorescent signals of the bacteria adherent to the implant were localized mostly at the distal end of the implant that was in contact with the distal physis of the femur (Fig. 3*A*). Histology showed marked reactive bony changes in the cortical, trabecular bone, and the physis, an abundance of mature neutrophils in the joint tissue (arthritis) and bone marrow cavity (osteomyelitis), and abscess formation within the marrow cavity of the cortex and distal end of the femur, all indicative of infection (Fig. 3*B*). These data suggest that the bacteria preferentially formed a biofilm on the implant at a site adjacent to the physis, and the abundance of neutrophils

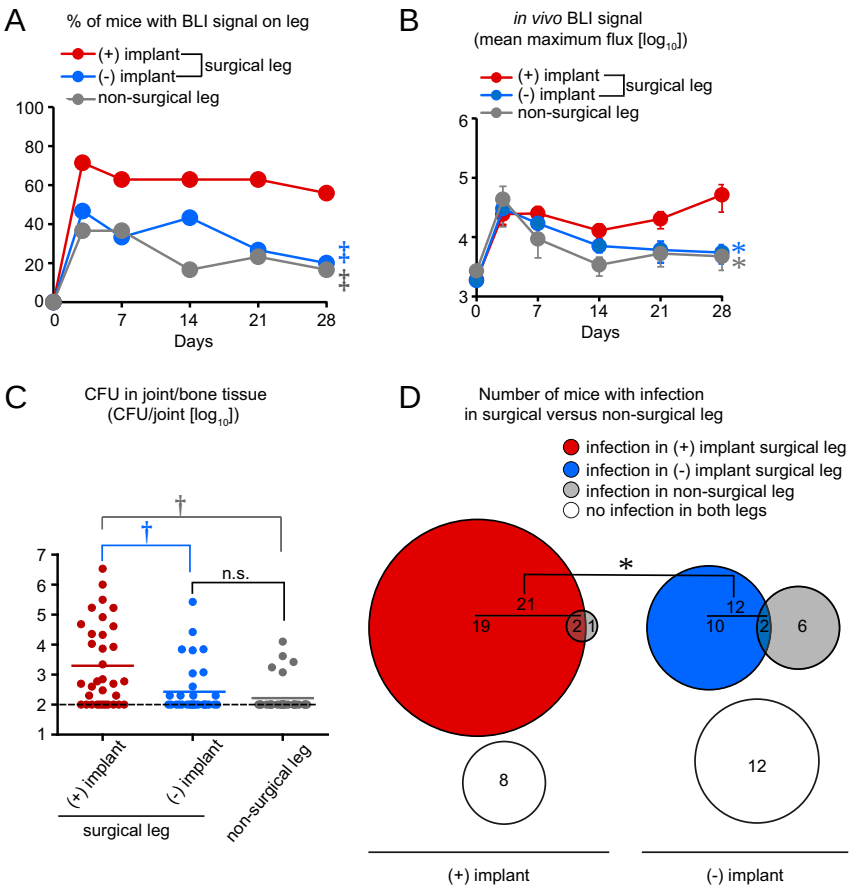

Fig. 2. Effect of the implant on the propensity for hematogenous infection. (*A*) Percentage of mice with detectable in vivo BLI signals from the indicated leg. (*B*) Mean in vivo BLI (mean maximum flux measured in photons·s^{-1}·cm^{-2} steradian ± SEM) from the indicated leg. (*C*) Ex vivo cfu; horizontal lines indicate geometric means. The limit of detection (horizontal dotted lines) was 100 cfu. (*D*) Euler diagram depicting the number of mice with and/or without infection (i.e., the presence and/or absence of ex vivo cfu) in the surgical and nonsurgical legs of mice with implants placed [(+) implant] vs. mice receiving sham surgery alone [(−) implant]. *$P < 0.05$, †$P < 0.01$, ‡$P < 0.001$, (+) implant surgical leg (red symbols) vs. (−) implant surgical leg (blue symbols) or nonsurgical leg (gray symbols), as measured by a two-way ANOVA performed on days 3–28 (*A*) or on days 7–28 (*B*), a two-tailed Mann–Whitney *U* test (*C*), or a two-tailed Fisher's exact test (*D*). Results are a compilation of four independent experiments ($n = 30$ mice per group). n.s., not significant.

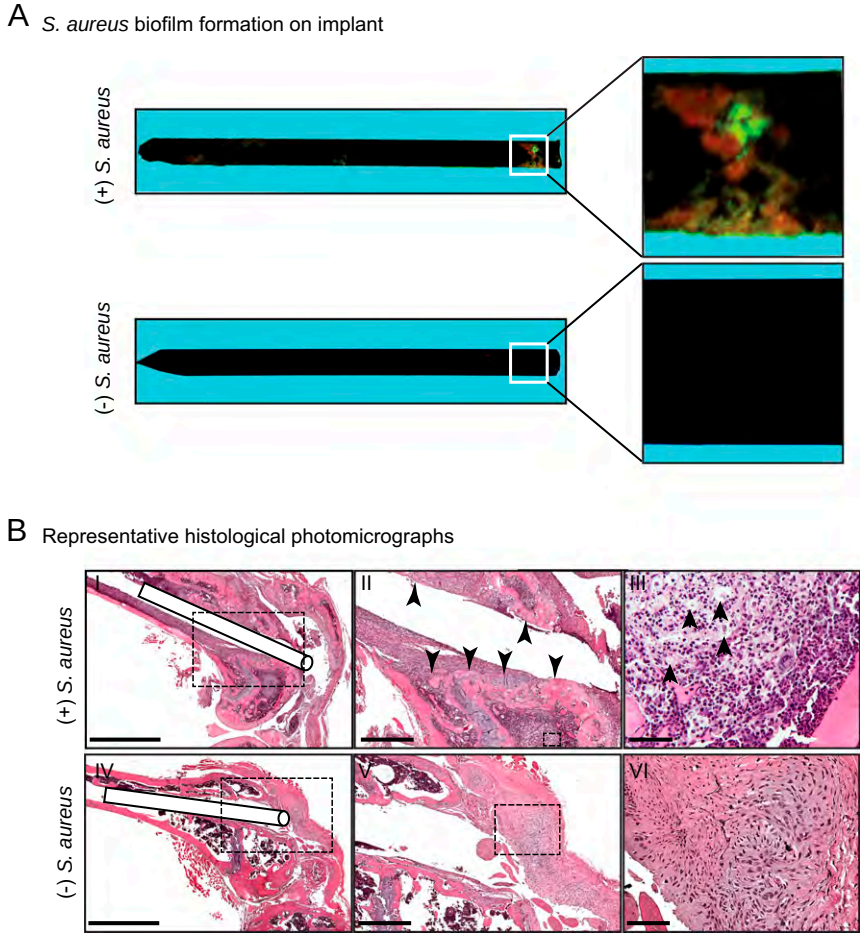

Fig. 3. Histopathology of the hematogenous implant infection. (*A*) Representative live/dead bacterial fluorescent stain of implants harvested on day 28 (green, live and dead bacteria; red, dead bacteria; yellow, merge) in one of three implants per group, with similar results. (Magnification: *Left*, 25×; *Right*, 200×.) (*B*) Representative photomicrographs of histologic sections from one of three mice per group, with similar results. (*I–III*) Infected knee joint with implant. (*I*) Low magnification (25×) with the line drawing of a cylinder representing the location of the implant within the femur. (*II*) Higher magnification (50×) of the boxed area in *I* showing bone proliferation of cortex and distal femoral physis (arrowheads) and osteomyelitis. (*III*) Higher magnification (400×) of the boxed area in *II* showing abscess formation within marrow space with mature neutrophils admixed with foamy macrophages (solid arrows). (*IV–VI*) Uninfected knee joint with implant only. (*IV*) Low magnification (25×) with the line drawing of a cylinder representing the location of the implant within the femur. (*V*) Higher magnification (50×) of the boxed area in *IV*. (*VI*) Higher magnification (200×) of the boxed area in *V* showing mild thickening of the patellar ligament at the distal end of the implant. (Scale bars: 2 mm in *B*, *I* and *IV*; 500 μm in *B*, *II* and *V*; 50 μm in *B*, *III*; and 100 μm in *B*, *VI*.)

in bone and joint tissue is consistent with the presence of both osteomyelitis and septic arthritis.

α-Toxin and Clumping Factor A Promote in Vitro Biofilm Formation. Next, we hypothesized that virulence factors involved in biofilm formation in vitro would contribute to the pathogenesis of the hematogenous orthopedic implant infection in vivo. Therefore, we first evaluated the effect of anti–α-toxin (AT) (MEDI4893*) and anti-clumping factor A (ClfA) (11H10) mAbs on in vitro biofilm formation. These mAbs are high-affinity, functional mAbs reported to reduce disease severity in various *S. aureus* disease models (32, 33). AT is a secreted pore-forming toxin (34) found to promote biofilm formation in vitro (35, 36) and to contribute to immune evasion in a murine model of orthopedic implant infection (37). ClfA is a surface-expressed fibrinogen-binding adhesin that has been shown to promote biofilm-like aggregations in synovial fluid (38) [providing a role for ClfA in septic arthritis (39, 40)] and is highly expressed in human orthopedic implant infections (41).

The anti-AT and anti-ClfA mAbs (0.5 μg/mL each) were first determined to have no effect, either alone or in combination, on the planktonic growth of NRS384 in broth culture (Fig. 4*A*). Using an established microtiter biofilm assay (42), the anti-AT and anti-ClfA mAbs (0.5 μg/mL each) were included alone and in combination at the beginning of the assay, and biofilm formation of NRS384 was assessed after 12 or 24 h. The anti-ClfA mAb and the anti-AT/ClfA mAb combination, but not the anti-AT mAb alone, inhibited biofilm formation after 12 and 24 h compared with an isotype control mAb (Fig. 4 *B* and *C*). In light of prior reports demonstrating that AT expression was associated with biofilm formation in vitro (35, 36), we evaluated the twofold mAb concentration (1 μg/mL). Again, neither mAb alone nor the mAb combination had any effect on the planktonic growth of NRS384 in broth culture (Fig. 4*D*). After 12 h, the anti-ClfA and anti-AT/ClfA mAb combination reduced biofilm formation significantly ($P < 0.05$), and there was a trend for the anti-AT mAb in inhibiting biofilm formation that approached statistical significance ($P = 0.058$) (Fig. 4*E*). After 24 h, anti-AT, anti-ClfA, and the anti-AT/anti-ClfA mAb combination all inhibited biofilm formation significantly ($P < 0.05$) (Fig. 4*F*). Thus, although the anti-AT mAb had a modest dose-dependent effect on in vitro biofilm formation, the anti-ClfA mAb had the greater effect and was responsible for a majority of the inhibition seen with the anti-AT/anti-ClfA combination.

mAbs Against AT and ClfA Reduce a Hematogenous Implant Infection in Vivo. To determine if the anti-AT and anti-ClfA mAbs would

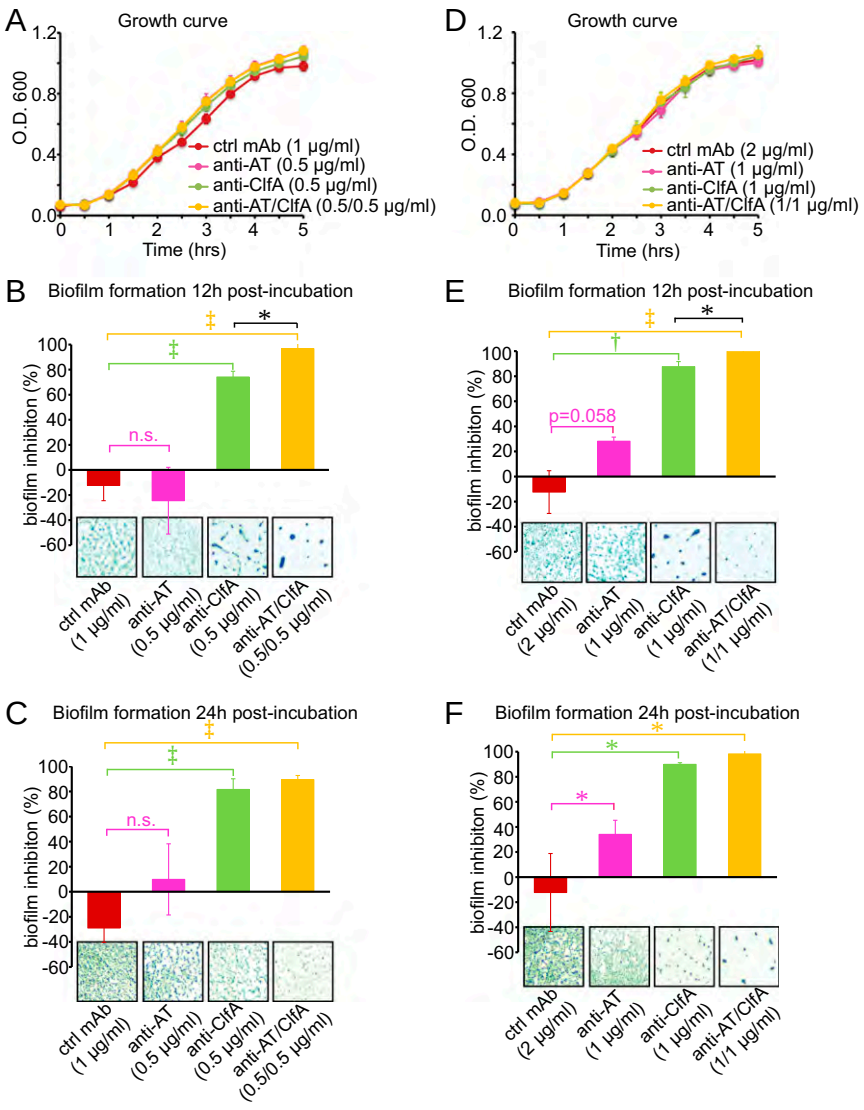

Fig. 4. Effect of anti-AT and anti-ClfA mAbs on in vitro biofilm formation. (*A* and *D*) OD_{600} of planktonic growth of NRS384 in broth culture in the presence of control (ctrl) mAb, anti-AT mAb, anti-ClfA mAb, or the anti-AT/anti-ClfA mAb combination at low (*A*) or high (*D*) mAb concentrations. (*B*, *C*, *E*, and *F*) Microtiter biofilm assay with NRS384 performed in the presence of control (ctrl) mAb, anti-AT mAb, anti-ClfA mAb, or the anti-AT/anti-ClfA mAb combination at low and high mAb concentrations for 12 h (*B* and *E*) and 24 h (*C* and *F*). Data are presented as the mean percentage of biofilm inhibition ± SEM in the wells with mAb added compared with wells without mAb added. *Insets* in *B*–*F* show representative photomicrographs of crystal violet-stained bacterial biofilm clusters on the bottom of the microtiter wells. (Magnification: 100×.) $^{*}P < 0.05$, $^{\dagger}P < 0.01$, $^{\ddagger}P < 0.001$, n.s., not significant vs. ctrl mAb as measured by a two-tailed Student's *t* test. Results are representative of two independent experiments ($n = 4$ replicate microtiter wells per group).

provide protection against an in vivo hematogenous implant infection, the mAbs were administered i.v. as single agents 1 d before i.v. *S. aureus* inoculation in the model of hematogenous orthopedic implant infection. Both the anti-AT mAb and the anti-ClfA mAb resulted in a significant decrease in the percentage of mice with in vivo BLI signal from the (+) implant surgical legs on days 3–28 ($P < 0.001$) (Fig. 5*A*). However, neither the anti-AT mAb nor the anti-ClfA mAb resulted in significant differences in the quantified in vivo BLI signals from the (+) implant surgical legs or ex vivo cfu from the surgical and nonsurgical legs on day 28 (Fig. 5 *B* and *C*). Thus, the individual mAbs reduced the propensity for the (+) implant surgical legs to become infected but did not alter the actual bacterial burden in the surgical or nonsurgical legs.

Given that the anti-AT and anti-ClfA mAbs exhibit distinct mechanisms of action and that each mAb decreased the percentage of mice with infection in the (+) implant surgical leg, and because we previously had seen improved activity of the mAb combination over monotherapy in a murine model of bacteremia (32), we evaluated the effect of targeting both AT and ClfA by administering the mAbs in combination. Prophylaxis with the anti-AT/anti-ClfA mAb combination significantly decreased the percentage of mice with in vivo BLI signals and reduced in vivo BLI signals in the (+) implant surgical leg compared with the control mAb on days 3–28 ($P < 0.05$) (Fig. 6 *A* and *B*). In addition, the anti-AT/anti-ClfA mAb combination significantly reduced ex vivo cfu from bone/joint tissue from the (+) implant surgical legs on day 28 as compared with the control mAb (Fig. 6*C*). To determine whether the anti-AT/anti-ClfA combination also impacted the propensity for the hematogenous implant infection, we evaluated the ex vivo cfu present in the surgical and nonsurgical legs of mice with (+) implant placement (Fig. 6*D*). The anti-AT/anti-ClfA mAb combination resulted in nearly a 50% reduction in the numbers of mice with infection in the (+) implant surgical legs compared with

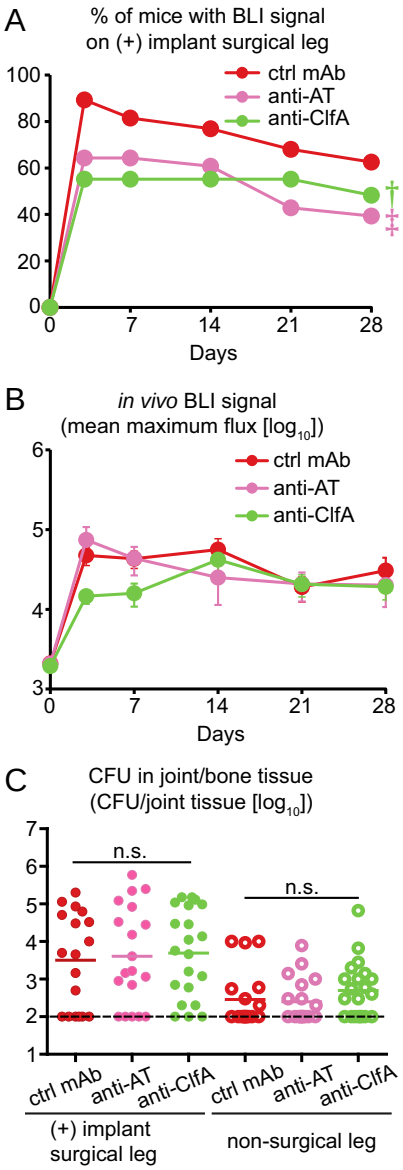

Fig. 5. Effect of anti-AT or anti-ClfA mAb prophylaxis against a hematogenous implant infection in vivo. At day −1 (1 d before i.v. bacterial inoculation) postsurgical mice with implants placed on day −21 were administered control (ctrl) mAb, anti-AT mAb, or anti-ClfA mAb (22.5 mg/kg, i.v.). (*A*) The percentage of mice with detectable in vivo BLI signals from the (+) implant surgical leg. (*B*) Mean in vivo BLI from the (+) implant surgical leg (mean maximum flux expressed as photons·s^{-1}·cm^{-2} steradian ± SEM). (*C*) Ex vivo cfu (solid horizontal lines indicate geometric means) from the (+) implant surgical leg and the nonsurgical leg; dotted horizontal dotted lines indicate the limit of detection (100 cfu). $^{\dagger}P < 0.01$, $^{\ddagger}P < 0.001$, vs. control mAb, as measured by a two-way ANOVA (performed on days 3–28) (*A* and *B*) or a two-tailed Mann–Whitney *U* test (*C*). Results are a compilation of five independent experiments ($n = 28$ mice per group). n.s., not significant.

the control mAb (11 vs. 20, respectively, $P < 0.05$). Moreover, the anti-AT/anti-ClfA mAb combination reduced the overall propensity of infection, because the numbers of mice with no detectable cfu in both the surgical and nonsurgical legs was increased twofold compared with the control mAb (15 vs. 7, respectively) ($P < 0.05$). Finally, we performed scanning electron microscopy to evaluate biofilm formation on the implants harvested at day 28. The implants from mice treated with the control mAb had dense biofilm aggregates, whereas the implants from mice treated with anti-AT/anti-ClfA combination therapy had only occasional coccoid bacteria (blue arrowheads in Fig. 6*E*) but lacked appreciable biofilm formation (white arrows in Fig. 6*E*). Taken together, a mAb combination targeting both AT and ClfA markedly reduced the hematogenous implant infection in vivo.

Discussion

S. aureus hematogenous implant infection is a major complication that impedes the long-term success of implantable medical devices and prostheses (9–11). Here we report the development of a mouse model of a hematogenous orthopedic implant infection using a virulent bioluminescent CA-MRSA strain (43) and in vivo whole-animal optical imaging to monitor the dynamics of the infection beginning with bacteremia and resulting in seeding and infection of the surgically placed implant and surrounding bone and joint tissue. This model provided several insights into factors that contribute to the pathogenesis of hematogenous orthopedic infections.

First, the BLI signals at early time points after i.v. challenge were disseminated throughout the internal organs of the mice, especially in the kidneys and bladder. However, as the infection progressed over the course of 28 d, the bacterial signals accumulated preferentially at the site of surgically implanted legs in most of the mice. In general, after a *S. aureus* i.v. challenge in mice, there is a predilection for the bacteria to cause a septic arthritis in the knee joints (27, 28). However, the presence of the orthopedic implant was a major determinant for the hematogenous implant infection, which occurred 70% of the time. Indeed, the number of mice with an infection in the (+) implant surgical leg was almost double the number of mice with an infection in the (−) implant surgical leg and almost three times the number with an infection in nonsurgical legs (Fig. 2*D*).

Second, the anatomical location where the bacteria seeded the implant, formed a biofilm, and caused an infection in the surrounding bone and joint tissue preferentially involved the area adjacent to the distal femoral physis. Although the precise reason for this anatomic location is unclear, the physis has an excellent blood supply from the metaphyseal vascular plexus fed by the metaphyseal arteries and adjacent vascularity consisting of the diaphyseal nutrient artery proximally, epiphyseal arteries distally, and capillary network from the perichondral arteries circumferentially. Therefore, it is likely that the bacteria in the blood hematogenously seeded the implant through this well-vascularized area. Alternatively (or in addition), the bacteria might have had a propensity to adhere to the implant and produce a biofilm at this location because of the continuous source of nutrients supplied by the direct and abundant blood flow to the physis. It should be noted that some of the mice did not develop a hematogenous implant infection, because on day 28 there were no detectable cfu from the implants or surrounding joint tissue of these mice. These mice also had reduced and eventually absent BLI signals at the surgical site at earlier time points. The reason for the lack of implant infection in some mice is unclear, but bacterial dissemination, biofilm formation, and proliferation at the surgical site are likely important determinants for the development of a persistent implant-related infection.

Third, fibronectin binding (in particular binding-enhancing polymorphisms in fibronectin-binding proteins A and B) was previously identified as an important pathogenic determinant for hematogenous implant infections involving cardiac devices in humans (44). However, a similar role for fibronectin binding was not found for hematogenous PJI in humans (45). To identify potential pathogenic factors that contributed to the hematogenous orthopedic implant infection in our mouse model, we investigated *S. aureus* AT and ClfA because they are involved in biofilm formation in vitro (35, 36) and in human synovial fluid specimens ex vivo (38) and have been implicated in septic arthritis (39, 40) and

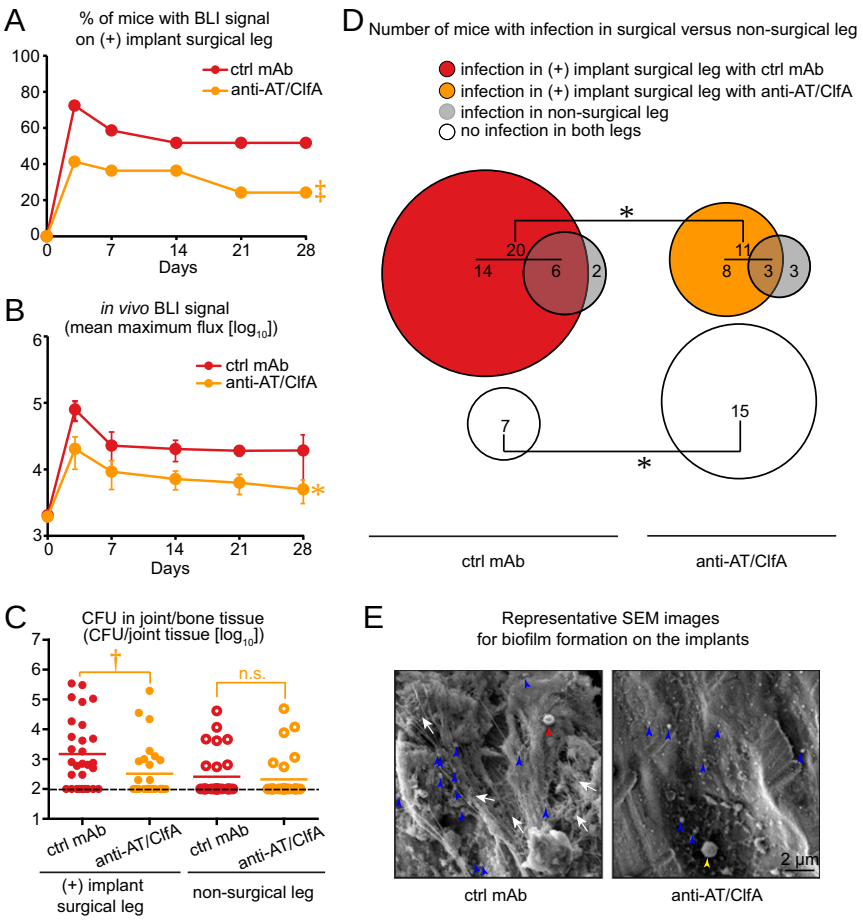

Fig. 6. Effect of anti-AT/anti-ClfA combination prophylaxis against a hematogenous implant infection in vivo. At day −1 (1 d before i.v. bacterial inoculation) postsurgical mice with implants placed on day −21 were administered control (ctrl) mAb (45 mg/kg) or the anti-AT/anti-ClfA mAb combination (22.5 mg/kg each, i.v.). (*A*) The percentage of mice with detectable in vivo BLI signals from the (+) implant surgical leg. (*B*) The mean in vivo BLI from the (+) implant surgical leg (mean maximum flux expressed as photons·s^{-1}·cm^{-2} steradian ± SEM). (*C*) Ex vivo cfu (solid horizontal lines indicated geometric means) from the (+) implant surgical leg and the nonsurgical leg; dotted horizontal lines indicate the limit of detection (100 cfu). (*D*) Euler diagram depicting the number of mice with and/or without infection (i.e., the presence and/or absence of ex vivo cfu) in the surgical and nonsurgical legs in mice treated with the control mAb vs. the anti-AT/ClfA mAb combination. (*E*) Representative scanning electron microscopy images of biofilm formation on implants harvested on day 28 (blue arrowheads indicate coccoid bacteria, white arrows indicate biofilm, the red arrowhead indicates a red blood cell, and the yellow arrowhead indicates a leukocyte). *$P < 0.05$, †$P < 0.01$, ‡$P < 0.001$, vs. control mAb, as measured by a two-way ANOVA (performed on days 3–28) (*A* and *B*), a two-tailed Mann-Whitney *U* test (*C*), or a two-tailed Fisher's exact test (*D*). Results for *A*–*D* are a compilation of four independent experiments ($n = 29$ mice per group). n.s., not significant.

primary orthopedic implant infections in mice and humans (37, 41). Neutralizing the activity of AT and ClfA with human anti-AT and anti-ClfA mAbs (32, 46) inhibited biofilm formation in vitro. The anti-ClfA mAb alone was a potent inhibitor of biofilm formation at both the low and high concentrations and at 12 and 24 h of the assay, whereas the anti-AT mAb significantly inhibited biofilm formation only at the high concentration and at 24 h of the assay. Moreover, neutralizing both AT and ClfA by using both mAbs in combination inhibited in vitro biofilm formation more effectively than neutralizing either AT or ClfA alone.

Finally, the anti-AT and anti-ClfA mAbs were evaluated alone and in combination in our model of hematogenous orthopedic implant infection. Prophylaxis with the anti-ClfA or anti-AT mAb alone modestly reduced the propensity of the infection but did not reduce the bacterial burden in the surgical or nonsurgical legs. In contrast, targeting both AT and ClfA with the anti-AT/anti-ClfA mAb combination resulted in more than a 50% reduction in the propensity for the hematogenous orthopedic implant infection, decreased bacterial burden in the (+) implant surgical legs, and reduced biofilm formation on the implants. Similar to the improved activity of the mAb combination reported in a murine model of bacteremia (32), the improved efficacy of the mAb combination in this model likely resulted from targeting complementary virulence mechanisms, including neutralization of AT-mediated tissue damage, inflammation and immune evasion, inhibition of ClfA-mediated fibrinogen binding and bacterial agglutination in the synovium (38), and anti-ClfA–mediated opsonophagocytic killing of *S. aureus* (32). In addition, AT has been shown to promote host cell lysis to provide a nutrient source for the bacteria in a model of *S. aureus* vaginal mucosal biofilm infection (47), and the inhibition of AT might have had a similar effect in our hematogenous implant-related biofilm infection.

Previous models of hematogenous orthopedic implant infections in rabbits and rats described the spread of the bacteremia infection to a surgically placed implant and surrounding bone and joint tissue but only at static time points after infection (29, 30). Other models studied bacteremia that resulted in septic arthritis in mice but in the absence of a surgically placed implant (27, 28). The present model of *S. aureus* hematogenous orthopedic infection represents an advance over these prior models because the recently developed bright bioluminescent *S. aureus* strain in combination with in vivo BLI provided an opportunity

to monitor the anatomic dissemination of the infection in the same animals noninvasively and longitudinally over time. Therefore, data regarding both the spatial and temporal spread of the hematogenous infection and the effect of anti-AT and anti-ClfA mAb therapy could be obtained.

This study has several limitations. First, the study was performed using a USA300 strain, which is the predominant *S. aureus* isolate that causes CA-MRSA infections in the United States. However, prior work found that USA200 *S. aureus* strains producing toxic shock syndrome toxin-1 (TSST-1) can cause hematogenous and osteomyelitis infections (48, 49). Because USA200 strains produce little or no AT because of a stop codon in the *AT* gene (50), the anti-AT mAb will likely not have an effect in USA200 or in other strains that do not produce AT. Future work will evaluate anti-ClfA mAb therapy in combination with mAbs against additional targets for broader coverage against USA200 and other *S. aureus* isolates. In addition, *S. aureus* superantigens, such as TSST-1, and certain cytolytic toxins, such as Panton–Valentine leukocidin, are important virulence factors in humans but have less involvement in mouse models (51). These and other differences between the species should be taken into account when translating our findings to humans.

Taken together, our results using a model of *S. aureus* hematogenous orthopedic infection that provided the opportunity for noninvasive and longitudinal monitoring of the dissemination of the bacteria from the bloodstream to the implant identified AT and ClfA as key pathogenic factors. In addition, given the marked efficacy of the human anti-AT/anti-ClfA mAb combination against the hematogenous implant infection, further preclinical testing and consideration of AT and ClfA as potential therapeutic targets is warranted. Our findings are particularly relevant because the demand for implantable medical devices is increasing, and targeted mAb-based prophylactic therapies could provide a feasible alternative to antibiotics to prevent or potentially treat hematogenous implant infections.

Methods

***S. aureus* Strain.** The bioluminescent SAP231 strain was used in all in vivo experiments and was generated as previously described from NRS384, a well-described USA300 CA-MRSA isolate obtained from a skin infection outbreak in the Mississippi prison system (43). SAP231 possesses a stably integrated modified *luxABCDE* operon from the bacterial insect pathogen *Photorhabdus luminescens*. Live and metabolically active SAP231 bacteria constitutively emit a blue-green light, which is maintained in all progeny without selection.

Bacterial Preparation. *S. aureus* bacteria were streaked onto tryptic soy agar (TSA) plates [tryptic soy broth (TSB, TSA plus 1.5% Bacto agar)] (BD Biosciences)] and grown overnight at 37 °C in a bacterial incubator. Single colonies were picked and cultured in TSB at 37 °C in a shaking incubator (MaxQ HP 420, ThermoFisher) (240 rpm) overnight (16 h), followed by a 1:50 subculture at 37 °C for 2 h to obtain midlogarithmic phase bacteria. The bacteria were pelleted, resuspended in sterile PBS, and washed two times. OD_{600} was measured to estimate the number of cfu, which was verified after overnight culture on TSA plates.

Mice. Ten- to twelve-week-old male C57BL/6 mice were used in all experiments. The mice were originally obtained from Jackson Laboratories and were bred and maintained under specific pathogen-free conditions at an American Association for the Accreditation of Laboratory Animal Care (AAALAC)-accredited animal facility at Johns Hopkins University and were housed according to procedures described in the *Guide for the Care and Use of Laboratory Animals* (52).

Mouse Model of a Hematogenous Orthopedic Infection. All procedures were approved by the Johns Hopkins University Animal Use and Care Committee. The surgical procedure was modified from previous work (26). Briefly, mice were anesthetized via inhalation isoflurane (2%), a skin incision was made over the right knee, and the distal right femur was accessed via a medial parapatellar arthrotomy with lateral displacement of the quadriceps–patellar complex. An intramedullary femoral canal was manually reamed with a 25-gauge needle, and an orthopedic-grade titanium K-wire (length 9 mm, diameter 0.6 mm) (Modern Grinding) was surgically placed in a retrograde fashion with 1 mm protruding into the knee joint space. The quadriceps–patellar complex was reduced to midline, and the surgical site was closed with absorbable Vicryl 5–0 sutures. For analgesia, sustained-release buprenorphine (2.5 mg/kg) was administered s.c. at the time of surgery. At 21 d postsurgery, SAP231 at three different inocula (1×10^6, 5×10^6, and 1.0×10^7 cfu) was inoculated i.v. via the retro-orbital vein. All mice with the 1×10^6 cfu and 5×10^6 cfu inoculum survived the bacterial challenge; the 1.0×10^7 cfu inoculum was the 10% lethal dose (LD_{10}), which resulted in slight differences in sample sizes between experiments.

In Vivo BLI. In vivo BLI was performed on anesthetized mice (2% isoflurane) using a Lumina III IVIS in vivo imaging system (PerkinElmer) and maximum flux (measured as photons·s^{-1}·cm^{-2} steradian) was measured within a 1×10^3-pixel circular region of interest using Living Image software (PerkinElmer) (limit of detection: 3.0×10^3 photons·s^{-1}·cm^{-2} steradian). The bioluminescent signals detected from the infected postsurgical site closely approximate the actual bacterial burden measured by the ex vivo cfu of homogenized bone/joint tissue as previously described (53, 54).

Ex Vivo cfu Counting. Mice were killed on day 28 post infection, and the peri-implant joint/bone tissue and implants from the surgical and nonsurgical legs were harvested as previously described (53, 54). Bacterial cfu were isolated by homogenizing the tissue (Pro200 Series homogenizer; Pro Scientific) in PBS on ice. Ex vivo cfu were counted after serially diluted joint/bone tissue homogenates were plated overnight on TSA plates.

Live/Dead Bacterial Staining and Histological Analysis. Mice were killed on day 28 post infection, and bone/joint specimens were obtained. The K-wire implants were removed by gently pulling the implant proximally so not to disturb the knee joint. Implants were stained using the LIVE/DEAD *Bac*Light Bacterial Viability Kit (Thermo Fisher) according to the manufacturer's recommendations, and green fluorescent signals (live and dead bacteria) and red fluorescent signals (dead bacteria) were visualized on a fluorescent microscope. All joint/bone tissue specimens were fixed in 10% formalin overnight, decalcified, and embedded in paraffin. Sagittal sections were cut at 4-μm thickness and then were stained with H&E for evaluation under light microscopy by a pathologist.

Anti-AT and Anti-ClfA mAbs. Anti-AT mAb (MEDI4893*), anti-ClfA (11H10), and control human IgG1 isotype [anti-HIV gp120 (R347)] mAbs are fully human antibodies that were generated as previously described (32, 46).

Planktonic Growth Assay. NRS384 bacteria were streaked onto TSA plates and grown overnight at 37 °C in a bacterial incubator. Single colonies were picked and cultured in TSB overnight (16 h) at 37 °C in a shaking incubator (240 rpm). The overnight culture then was diluted to an OD_{600} of 0.1 in fresh TSB containing anti-AT mAb, anti-ClfA mAb, the anti-AT/ClfA mAb combination at low (0.5 μg/mL) and high (1.0 μg/mL) concentrations, or an isotype control mAb (1 or 2 μg/mL, respectively). The OD_{600} was measured every 30 min for 5 h.

Microtiter Biofilm Assay. The in vitro microtiter biofilm assay was performed according to previously described methods (42). Briefly, the NRS384 strain was grown in TSB for 16 h at 240 rpm. The overnight culture then was diluted with fresh TSB supplemented with 3% NaCl and 0.5% glucose, and the bacterial concentration was adjusted to an OD_{600} of 0.1. The bacteria were grown in TSB supplemented with 3% NaCl and 0.5% glucose in plasma-coated 96-well microtiter plates (Corning) with the addition of anti-AT mAb, anti-ClfA mAb, the anti-AT/anti-ClfA mAb combination at low (0.5 μg/mL) and high (1.0 μg/mL) concentrations, or an isotype control mAb (1 or 2 μg/mL), or without mAb added. Bacterial biofilm formation was detected after three washings with PBS, fixing with ethanol (100%), staining with crystal violet, three additional washings with double-distilled H_2O, destaining with acetic acid (33%), and reading the OD_{580}. Data are presented as the percent of biofilm inhibition as calculated by the formula [(OD_{580} without mAb) − (OD_{580} of each mAb)]/(OD_{580} without mAb) × 100.

Scanning Electron Microscopy. K-wire implants were removed from the femurs at 28 d after bacterial inoculation and were fixed in buffered 4% formaldehyde/2.5% glutaraldehyde solution overnight (16 h). All K-wire samples were postfixed in 1% osmium tetraoxide in PBS for 2 h followed by subsequent dehydration in a graded ethanol series. Samples then were placed into transitional series of graded ethanol:hexamethyldisilazane (HMDS) mixtures (2:1, 1:1, and 1:2; each for 30 min), and finally into pure HMDS (twice, 30 min each). Specimens were air-dried in a chemical hood before

sputter-coating with a gold-palladium alloy and were imaged using a field-emission scanning electron microscope (JSM-6700F FE-SEM; JEOL).

Statistics. Data were compared using a two-way ANOVA, two-tailed Mann–Whitney *U* test, two-tailed Student's *t* test, or two-tailed Fisher exact test, as indicated in the figure legends. All statistical analyses were calculated using Prism software (GraphPad). Data are presented as mean ± SEM, and values of $P < 0.05$ were considered statistically significant.

ACKNOWLEDGMENTS. This work was supported by a sponsored research agreement from MedImmune, LLC through a Johns Hopkins-MedImmune Academic Industry Partnership.

1. Hall-Stoodley L, Costerton JW, Stoodley P (2004) Bacterial biofilms: From the natural environment to infectious diseases. *Nat Rev Microbiol* 2:95–108.
2. Costerton JW, Stewart PS, Greenberg EP (1999) Bacterial biofilms: A common cause of persistent infections. *Science* 284:1318–1322.
3. del Pozo JL, Patel R (2007) The challenge of treating biofilm-associated bacterial infections. *Clin Pharmacol Ther* 82:204–209.
4. Darouiche RO (2004) Treatment of infections associated with surgical implants. *N Engl J Med* 350:1422–1429.
5. Osmon DR, et al.; Infectious Diseases Society of America (2013) Diagnosis and management of prosthetic joint infection: Clinical practice guidelines by the Infectious Diseases Society of America. *Clin Infect Dis* 56:e1–e25.
6. Parvizi J, et al. (2015) Novel developments in the prevention, diagnosis, and treatment of periprosthetic joint infections. *J Am Acad Orthop Surg* 23:S32–S43.
7. Del Pozo JL, Patel R (2009) Clinical practice. Infection associated with prosthetic joints. *N Engl J Med* 361:787–794.
8. Zimmerli W, Trampuz A, Ochsner PE (2004) Prosthetic-joint infections. *N Engl J Med* 351:1645–1654.
9. Tande AJ, et al. (2016) Clinical presentation, risk factors, and outcomes of hematogenous prosthetic joint infection in patients with *Staphylococcus aureus* bacteremia. *Am J Med* 129:221.e11–221.e20.
10. Konigsberg BS, Della Valle CJ, Ting NT, Qiu F, Sporer SM (2014) Acute hematogenous infection following total hip and knee arthroplasty. *J Arthroplasty* 29:469–472.
11. Sendi P, Banderet F, Graber P, Zimmerli W (2011) Periprosthetic joint infection following *Staphylococcus aureus* bacteremia. *J Infect* 63:17–22.
12. Kourbatova EV, et al. (2005) Emergence of community-associated methicillin-resistant *Staphylococcus aureus* USA 300 clone as a cause of health care-associated infections among patients with prosthetic joint infections. *Am J Infect Control* 33:385–391.
13. Peel TN, Cheng AC, Buising KL, Choong PF (2012) Microbiological aetiology, epidemiology, and clinical profile of prosthetic joint infections: Are current antibiotic prophylaxis guidelines effective? *Antimicrob Agents Chemother* 56:2386–2391.
14. Murdoch DR, et al. (2001) Infection of orthopedic prostheses after *Staphylococcus aureus* bacteremia. *Clin Infect Dis* 32:647–649.
15. Sakoulas G, Moellering RC, Jr (2008) Increasing antibiotic resistance among methicillin-resistant *Staphylococcus aureus* strains. *Clin Infect Dis* 46:S360–S367.
16. van Hal SJ, Fowler VG, Jr (2013) Is it time to replace vancomycin in the treatment of methicillin-resistant *Staphylococcus aureus* infections? *Clin Infect Dis* 56:1779–1788.
17. Marculescu CE, Osmon DR (2005) Antibiotic prophylaxis in orthopedic prosthetic surgery. *Infect Dis Clin North Am* 19:931–946.
18. Mazur DJ, Fuchs DJ, Abicht TO, Peabody TD (2015) Update on antibiotic prophylaxis for genitourinary procedures in patients with artificial joint replacement and artificial heart valves. *Urol Clin North Am* 42:441–447.
19. Watters W, 3rd, et al.; American Academy of Orthopedic Surgeons; American Dental Association (2013) Prevention of orthopaedic implant infection in patients undergoing dental procedures. *J Am Acad Orthop Surg* 21:180–189.
20. Teillant A, Gandra S, Barter D, Morgan DJ, Laxminarayan R (2015) Potential burden of antibiotic resistance on surgery and cancer chemotherapy antibiotic prophylaxis in the USA: A literature review and modelling study. *Lancet Infect Dis* 15:1429–1437.
21. Goff DA, et al. (2017) A global call from five countries to collaborate in antibiotic stewardship: United we succeed, divided we might fail. *Lancet Infect Dis* 17:e56–e63.
22. Nishitani K, et al. (2015) Quantifying the natural history of biofilm formation in vivo during the establishment of chronic implant-associated *Staphylococcus aureus* osteomyelitis in mice to identify critical pathogen and host factors. *J Orthop Res* 33: 1311–1319.
23. Prabhakara R, Harro JM, Leid JG, Harris M, Shirtliff ME (2011) Murine immune response to a chronic *Staphylococcus aureus* biofilm infection. *Infect Immun* 79: 1789–1796.
24. Heim CE, et al. (2014) Myeloid-derived suppressor cells contribute to *Staphylococcus aureus* orthopedic biofilm infection. *J Immunol* 192:3778–3792.
25. Inzana JA, Schwarz EM, Kates SL, Awad HA (2015) A novel murine model of established Staphylococcal bone infection in the presence of a fracture fixation plate to study therapies utilizing antibiotic-laden spacers after revision surgery. *Bone* 72: 128–136.
26. Pribaz JR, et al. (2012) Mouse model of chronic post-arthroplasty infection: Noninvasive in vivo bioluminescence imaging to monitor bacterial burden for long-term study. *J Orthop Res* 30:335–340.
27. Verdrengh M, Tarkowski A (1997) Role of neutrophils in experimental septicemia and septic arthritis induced by *Staphylococcus aureus*. *Infect Immun* 65:2517–2521.
28. Corrado A, et al. (2016) *Staphylococcus aureus*-dependent septic arthritis in murine knee joints: Local immune response and beneficial effects of vaccination. *Sci Rep* 6: 38043.
29. Poultsides LA, et al. (2008) Novel model for studying hematogenous infection in an experimental setting of implant-related infection by a community-acquired methicillin-resistant *S. aureus* strain. *J Orthop Res* 26:1355–1362.
30. Shiels SM, Bedigrew KM, Wenke JC (2015) Development of a hematogenous implant-related infection in a rat model. *BMC Musculoskelet Disord* 16:255.
31. McDougal LK, et al. (2003) Pulsed-field gel electrophoresis typing of oxacillin-resistant *Staphylococcus aureus* isolates from the United States: Establishing a national database. *J Clin Microbiol* 41:5113–5120.
32. Tkaczyk C, et al. (2016) Targeting alpha toxin and ClfA with a multimechanistic monoclonal-antibody-based approach for prophylaxis of serious *Staphylococcus aureus* disease. *MBio* 7:e00528-16.
33. Hua L, et al. (2014) Assessment of an anti-alpha-toxin monoclonal antibody for prevention and treatment of *Staphylococcus aureus*-induced pneumonia. *Antimicrob Agents Chemother* 58:1108–1117.
34. Berube BJ, Bubeck Wardenburg J (2013) *Staphylococcus aureus* α-toxin: Nearly a century of intrigue. *Toxins (Basel)* 5:1140–1166.
35. Caiazza NC, O'Toole GA (2003) Alpha-toxin is required for biofilm formation by *Staphylococcus aureus*. *J Bacteriol* 185:3214–3217.
36. den Reijer PM, et al. (2016) Detection of alpha-toxin and other virulence factors in biofilms of *Staphylococcus aureus* on polystyrene and a human epidermal model. *PLoS One* 11:e0145722, and erratum (2016) 11:e0152544.
37. Scherr TD, et al. (2015) *Staphylococcus aureus* biofilms induce macrophage dysfunction through leukocidin AB and alpha-toxin. *MBio* 6:e01021-15.
38. Dastgheyb S, Parvizi J, Shapiro IM, Hickok NJ, Otto M (2015) Effect of biofilms on recalcitrance of staphylococcal joint infection to antibiotic treatment. *J Infect Dis* 211: 641–650.
39. Josefsson E, Hartford O, O'Brien L, Patti JM, Foster T (2001) Protection against experimental *Staphylococcus aureus* arthritis by vaccination with clumping factor A, a novel virulence determinant. *J Infect Dis* 184:1572–1580.
40. Palmqvist N, Foster T, Fitzgerald JR, Josefsson E, Tarkowski A (2005) Fibronectin-binding proteins and fibrinogen-binding clumping factors play distinct roles in staphylococcal arthritis and systemic inflammation. *J Infect Dis* 191:791–798.
41. Post V, et al. (2014) Phenotypic and genotypic characterisation of *Staphylococcus aureus* causing musculoskeletal infections. *Int J Med Microbiol* 304:565–576.
42. Hammer ND, et al. (2014) Inter- and intraspecies metabolite exchange promotes virulence of antibiotic-resistant *Staphylococcus aureus*. *Cell Host Microbe* 16:531–537.
43. Plaut RD, Mocca CP, Prabhakara R, Merkel TJ, Stibitz S (2013) Stably luminescent *Staphylococcus aureus* clinical strains for use in bioluminescent imaging. *PLoS One* 8: e59232.
44. Hos NJ, et al. (2015) Amino acid alterations in fibronectin binding protein A (FnBPA) and bacterial genotype are associated with cardiac device related infection in *Staphylococcus aureus* bacteraemia. *J Infect* 70:153–159.
45. Eichenberger EM, et al. (2015) Polymorphisms in fibronectin binding proteins A and B among *Staphylococcus aureus* bloodstream isolates are not associated with arthroplasty infection. *PLoS One* 10:e0141436.
46. Tkaczyk C, et al. (2012) Identification of anti-alpha toxin monoclonal antibodies that reduce the severity of *Staphylococcus aureus* dermonecrosis and exhibit a correlation between affinity and potency. *Clin Vaccine Immunol* 19:377–385.
47. Anderson MJ, et al. (2012) Alpha-toxin promotes *Staphylococcus aureus* mucosal biofilm formation. *Front Cell Infect Microbiol* 2:64.
48. Abdelnour A, Bremell T, Tarkowski A (1994) Toxic shock syndrome toxin 1 contributes to the arthritogenicity of *Staphylococcus aureus*. *J Infect Dis* 170:94–99.
49. Loughran AJ, et al. (2016) Impact of sarA and phenol-soluble modulins on the pathogenesis of osteomyelitis in diverse clinical isolates of *Staphylococcus aureus*. *Infect Immun* 84:2586–2594.
50. Lin YC, et al. (2011) Proinflammatory exoprotein characterization of toxic shock syndrome *Staphylococcus aureus*. *Biochemistry* 50:7157–7167.
51. Salgado-Pabón W, Schlievert PM (2014) Models matter: The search for an effective *Staphylococcus aureus* vaccine. *Nat Rev Microbiol* 12:585–591.
52. National Research Council (2011) *Guide for the Care and Use of Laboratory Animals* (National Academies Press, Washington, DC), 8th Ed.
53. Niska JA, et al. (2013) Vancomycin-rifampin combination therapy has enhanced efficacy against an experimental *Staphylococcus aureus* prosthetic joint infection. *Antimicrob Agents Chemother* 57:5080–5086.
54. Niska JA, et al. (2012) Daptomycin and tigecycline have broader effective dose ranges than vancomycin as prophylaxis against a *Staphylococcus aureus* surgical implant infection in mice. *Antimicrob Agents Chemother* 56:2590–2597.